Optically controlled polarizer using a ladder transition for high speed Stokesmetric Imaging and Quantum Zeno Effect based optical logic

Subramanian Krishnamurthy,[1] Y. Wang,[1] Y. Tu,[1] S. Tseng,[1] and M.S. Shahriar[1,2,*]

[1]*Department of EECS, Northwestern University, Evanston, IL 60208, USA*
[2]*Department of Physics and Astronomy, Northwestern University, Evanston, IL 60208, USA*
[*]*shahriar@northwestern.edu*

Abstract: We demonstrate an optically controlled polarizer at ~1323 nm using a ladder transition in a Rb vapor cell. The lower leg of the $5S_{1/2}$,F = 1->$5P_{1/2}$,F = 1,2->$6S_{1/2}$,F = 1,2 transitions is excited by a Ti:Sapphire laser locked to a saturated absorption signal, representing the control beam. A tunable fiber laser at ~1323 nm is used to excite the upper leg of the transitions, representing the signal beam. When the control beam is linearly polarized, it produces an excitation of the intermediate level with a particular orientation of the angular momentum. Under ideal conditions, this orientation is transparent to the signal beam if it has the same polarization as the control beam and is absorbed when it is polarized orthogonally. We also present numerical simulations of the system using a comprehensive model which incorporates all the relevant Zeeman sub-levels in the system, and identify means to improve the performance of the polarizer. A novel algorithm to compute the evolution of large scale quantum system enabled us to perform this computation, which may have been considered too cumbersome to carry out previously. We describe how such a polarizer may serve as a key component for high-speed Stokesmetric imaging. We also show how such a polarizer, combined with an optically controlled waveplate, recently demonstrated by us, can be used to realize a high speed optical logic gate by making use of the Quantum Zeno Effect. Finally, we describe how such a logic gate can be realized at an ultra-low power level using a tapered nanofiber embedded in a vapor cell.

OCIS codes: (020.4180) Multiphoton processes; (020.1670) Coherent optical effects.

References and links

1. S. E. Harris and Y. Yamamoto, "Photon switching by quantum interference," Phys. Rev. Lett. **81**(17), 3611–3614 (1998).
2. R. G. Beausoleil, W. J. Munro, D. A. Rodrigues, and T. P. Spiller, "Applications of electromagnetically induced transparency to quantum information processing," J. Mod. Opt. **51**(16-18), 2441–2448 (2004).
3. A. M. C. Dawes, L. Illing, S. M. Clark, and D. J. Gauthier, "All-optical switching in Rubidium vapor," Science **308**(5722), 672–674 (2005).
4. M. Bajcsy, S. Hofferberth, V. Balic, T. Peyronel, M. Hafezi, A. S. Zibrov, V. Vuletic, and M. D. Lukin, "Efficient All-optical switching using slow light within a hollow Fiber," Phys. Rev. Lett. **102**(20), 203902 (2009).
5. V. Venkataraman, P. Londero, A. R. Bhagwat, A. D. Slepkov, and A. L. Gaeta, "All-optical modulation of four-wave mixing in an Rb-filled photonic bandgap fiber," Opt. Lett. **35**(13), 2287–2289 (2010).
6. K. Salit, M. Salit, S. Krishnamurthy, Y. Wang, P. Kumar, and M. S. Shahriar, "Ultra-low power, Zeno effect based optical modulation in a degenerate V-system with a tapered nano fiber in atomic vapor," Opt. Express **19**(23), 22874–22881 (2011).
7. S. Krishnamurthy, Y. Wang, Y. Tu, S. Tseng, and M. S. Shahriar, "High efficiency optical modulation at a telecom wavelength using the quantum Zeno effect in a ladder transition in Rb atoms," Opt. Express **20**(13), 13798–13809 (2012).

#194534 - $15.00 USD Received 24 Jul 2013; revised 11 Sep 2013; accepted 14 Sep 2013; published 7 Oct 2013

8. S. Krishnamurthy, Y. Wang, Y. Tu, S. Tseng, and M. S. Shahriar, "Optically controlled waveplate at a telecom wavelength for all-optical switching," Preprint, http://lapt.ece.northwestern.edu/preprints/waveplate.pdf.
9. S. M. Spillane, G. S. Pati, K. Salit, M. Hall, P. Kumar, R. G. Beausoleil, and M. S. Shahriar, "Observation of nonlinear optical interactions of ultralow levels of light in a tapered optical nanofiber embedded in a hot Rubidium vapor," Phys. Rev. Lett. **100**(23), 233602 (2008).
10. G. Brambilla, V. Finazzi, and D. J. Richardson, "Ultra-low-loss optical fiber nanotapers," Opt. Express **12**(10), 2258–2263 (2004).
11. S. M. Hendrickson, M. M. Lai, T. B. Pittman, and J. D. Franson, "Observation of two-photon absorption at low power levels using tapered optical fibers in Rubidium vapor," Phys. Rev. Lett. **105**(17), 173602 (2010).
12. T. Nee and S. F. Nee, "Infrared polarization signatures for targets," Proc. SPIE **2469**, 231–241 (1995).
13. S. Y. Lu and R. A. Chipman, "Interpretation of Mueller matrices based on polar decomposition," J. Opt. Soc. Am. A **13**(5), 1106–1113 (1996).
14. X. Liu, S. C. Tseng, R. Tripathi, A. Heifetz, S. Krishnamurthy, and M. S. Shahriar, "White light interferometric detection of unpolarized light for complete Stokesmetric optical coherence tomography," Opt. Commun. **284**(14), 3497–3503 (2011).
15. X. Liu, A. Heifetz, S. C. Tseng, and M. S. Shahriar, "High-speed inline holographic Stokesmeter imaging," Appl. Opt. **48**(19), 3803–3808 (2009).
16. B. Misra and E. C. G. Sudarshan, "The Zeno's paradox in quantum theory," J. Math. Phys. **18**(4), 756–763 (1977).
17. W. M. Itano, D. J. Heinzen, J. J. Bollinger, and D. J. Wineland, "Quantum Zeno Effect," Phys. Rev. A **41**(5), 2295–2300 (1990).
18. Y. Huang, J. B. Altepeter, and P. Kumar, "Interaction-free all-optical switching via the quantum Zeno effect," Phys. Rev. A **82**(6), 063826 (2010).
19. S. Weilandy, L. Alexander, and L. Gaeta, "Coherent control of the polarization of an optical field," Phys. Rev. Lett. **81**(16), 3359–3362 (1998).
20. M. Xiao, Y. Li, S. Jin, and J. Gea-Banacloche, "Measurement of dispersive properties of electromagnetically induced transparency of Rubidium atoms," Phys. Rev. Lett. **74**(5), 666–669 (1995).
21. P. J. Curran, "Polarized visible light as an aid to vegetation classification," Remote Sens. Environ. **12**(6), 491–499 (1982).
22. M. J. Duggin, "Imaging polarimetry in scene element discrimination," Proc. SPIE **3754**, 108–117 (1999).
23. B. J. DeBoo, J. M. Sasian, and R. A. Chipman, "Depolarization of diffusely reflecting man-made objects," Appl. Opt. **44**(26), 5434–5445 (2005).
24. J. F. de Boer, T. E. Milner, and J. S. Nelson, "Determination of the depth-resolved Stokes parameters of light backscattered from turbid media by use of polarization-sensitive optical coherence tomography," Opt. Lett. **24**(5), 300–302 (1999).
25. D. A. Steck, "Alkali D line data," http://steck.us/alkalidata/rubidium87numbers.pdf.
26. M. S. Shahriar, Y. Wang, S. Krishnamurthy, Y. Tu, G. S. Pati, and S. Tseng, "Evolution of an N-level system via automated vectorization of the Liouville equations and application to optically controlled polarization rotation," Prepint, http://arxiv.org/abs/1309.1130.
27. D. Stokes, *Principles and Practice of Variable Pressure/Environmental Scanning Electron Microscopy* (John Wiley & Sons, 2008), Chap. 8.

1. Introduction

All-optical logic gates are important for quantum information processing [1–5]. Conventional techniques of non-linear optics typically require relatively high power, and are not well suited for these applications. An ultra-low power Quantum Zeno Effect (QZE) based optical modulator using a degenerate V-system and a tapered nano fiber embedded in Rb vapor has recently been demonstrated by us [6]. We also demonstrated the ladder type Zeno modulator and proposed a novel scheme (employing high pressure buffer gas to broaden the atomic transitions) for a high-speed modulator (tens of GHz) that can be used to modulate signals at 1323 nm, using a control beam at 795 nm [7]. Recently, we have also shown [8] how an optically controlled waveplate employing a ladder transition can be used to realize a directional switch, as required in any telecommunication switching network. Here, we show that when such a switch is augmented by the addition of an optically controlled polarizer, the system exhibits ideal QZE, and leads to an optical logic gate. We also demonstrate experimentally the realization of such a polarizer using a ladder transition in Rb. In combination with a tapered nano fiber (TNF) setup [6, 9–11], this approach can be used to produce an optical logic gate at extremely low powers of the control beam (~40nW). The optically controlled polarizer, in combination with the optically controlled waveplate, could also be used for high speed Stokesmetric Imaging (SI) [12–15].

#194534 - $15.00 USD Received 24 Jul 2013; revised 11 Sep 2013; accepted 14 Sep 2013; published 7 Oct 2013

The rest of the paper is organized as follows. In section 2, we present an overview of the QZE. In section 3, we present an ideal mechanism to produce an optically controlled polarizer using ladder transition in Rb. A schematic of how such a polarizer and an optically controlled waveplate can be used to produce an optical logic gate based on the QZE is discussed in section 4. In section 5, we briefly describe a typical scenario in SI and how an optically controlled polarizer is useful. In section 6, we present details regarding experimental set-up and discuss non-idealities in the experiment. Experimental results are presented in section 7. In section 8, we describe the comprehensive model used in our numerical simulation which incorporates all the relevant Zeeman sub-levels in the system. In section 9, we provide an outlook about future work that will be pursued and in section 10, we present our conclusions. Finally, we have also included an appendix under section 11 where we provide some insight into differences in absorption lineshapes when operating under co- and counter-propagating geometry in a cascade system.

2. Quantum Zeno effect (QZE)

The quantum Zeno effect (QZE) [16–18] is the suppression of the evolution of a quantum state through the quantum measurement process. Figure 1(a) shows the energy level diagram of a three level system that illustrates this process. Here, states |1> and |2> are assumed long-lived, while state |3> decays rapidly, at a rate Γ, into state |1> only. The QZE in this configuration can be described as follows. In the absence of any coupling to state |3>, state |1> will undergo Rabi oscillation, thus getting excited to state |2> at a rate determined by the 1↔2 coupling strength. When coupled to state |3>, the spontaneous emission emulates a measurement process, which resets the quantum state of the system to state |1>. As such, evolution of state |1> into state |2> is inhibited.

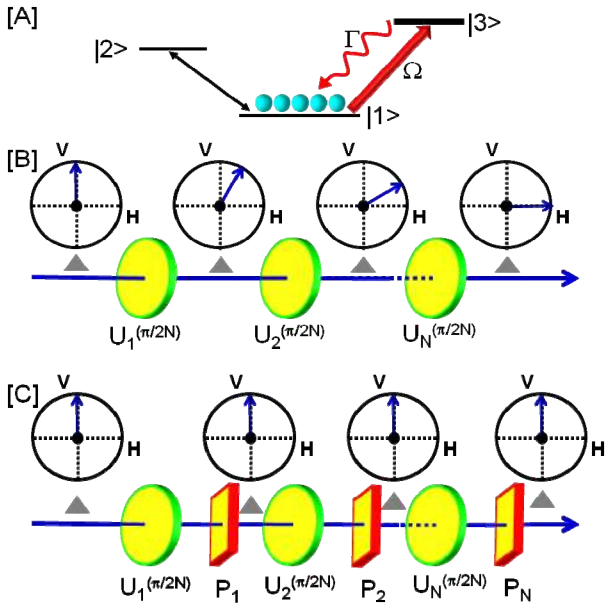

Fig. 1. [A] Quantum Zeno Efffect in an atomic V-system. [B] Evolution of the quantum state of a photon via passage through a series of waveplates. [C] In the presence of interleaved polarizers acting as measurement devices, the evolution to the horizontally polarized state is inhibited.

The phenomenon described above, although initially investigated in the context of atomic transitions, is in fact a general quantum mechanical effect occurring in any system where periodic quantum measurement and quantum state evolution occur. In particular, it is

#194534 - $15.00 USD Received 24 Jul 2013; revised 11 Sep 2013; accepted 14 Sep 2013; published 7 Oct 2013

instructive to analyze a bulk-optic model for this effect, as illustrated in Fig. 1(b). Here, we consider the evolution of the polarization state of a photon. The polarization degree of freedom for the photon spans two orthogonal states: $|V\rangle$ and $|H\rangle$ representing vertical and horizontal polarizations, respectively. The general quantum state can thus be written as $\alpha|V\rangle+\beta|H\rangle$, with $|\alpha|^2+|\beta|^2=1$. Consider now a specific situation where input quantum state is $|V\rangle$. When it passes through a wave plate with its fast/slow axis at an angle of 45° with respect to the vertical axis, the polarization state of the photon can be expressed as (ignoring an overall phase factor) $|\psi\rangle=\cos(\Delta nwt/2)|V\rangle+i\sin(\Delta nwt/2)|H\rangle$,. where Δn is the difference in refractive index between the fast and slow axis of the waveplate, t is the time of propagation and ω is the optical frequency. We can describe this process by an unitary evolution operator U_ϕ such that $U_\phi|V\rangle=\cos\phi|V\rangle+\sin\phi|H\rangle$, where $\phi = \Delta n\omega t/2$. When N such plates are placed in series, each causing a unitary evolution U_ϕ with $\phi = \pi/2N$, the polarization state of the photon at the output become $|H\rangle$, aside from an overall but inconsequential phase factor. Consider next a situation where these waveplates are interleaved with polarizers oriented along the vertical axis, as shown in Fig. 1(c). The polarizers act as a measurement device, collapsing the state to be $|V\rangle$ with probability $\cos^2\phi$. In the limit $N\to\infty$, corresponding to continuous measurement, the final state will be the same as the initial state.

It is also instructive to analyze this process without invoking a quantum description of light. Specifically, we consider a classical light beam polarized in the $\hat{x}$ (vertical) direction at the input. After passing through a waveplate, the polarization state can be expressed as $\alpha\hat{x}+\beta\hat{y}$, with $|\alpha|^2+|\beta|^2=1$, and $\alpha=\cos(\pi/2N)$. It is now easy to see that after a series of N waveplates and polarizers, the output intensity can be expressed as $I_{out} = I_0\,[\cos^2(\pi/2N)]^N$ and in the limit $N\to\infty$, it can be verified that $I_{out}\to I_0$, where I_0 is the initial intensity. This result seems to imply that there is a so-called "classical Zeno effect". This is erroneous, since the concept of a measurement induced reduction of a state is absent in the classical World. Instead, the process can be understood via the Quantum Zeno effect by considering a quantum model of a classical laser field (by which we mean a field with intensity much stronger than that of a single photon). Any such field (including, but not limited to the coherent state) can be expressed as a superposition of the Fock states: $|V\rangle=\sum_n \alpha|n\rangle$. Now, the analysis we presented above for a single photon can be applied to each Fock state. Thus, after passing though the series of N polarizers and waveplates, the polarization state remains the same. Therefore, QZE applies even if one does not explicitly consider the optical field quantum mechanically.

3. Optically controlled polarizer

It is well known that the polarization state of an optical field gets modified after propagating through an optically dense vapor medium, a manifestation of optical activity. In an atomic system involving ladder type transitions, the presence of two different frequencies open up the possibility of controlling the behavior of the probe (upper leg) polarization by careful design of the pump parameters (lower leg). In particular, it is possible to make the vapor cell act as a polarizer, oriented either vertically or horizontally depending on the polarization of the pump.

#194534 - $15.00 USD Received 24 Jul 2013; revised 11 Sep 2013; accepted 14 Sep 2013; published 7 Oct 2013

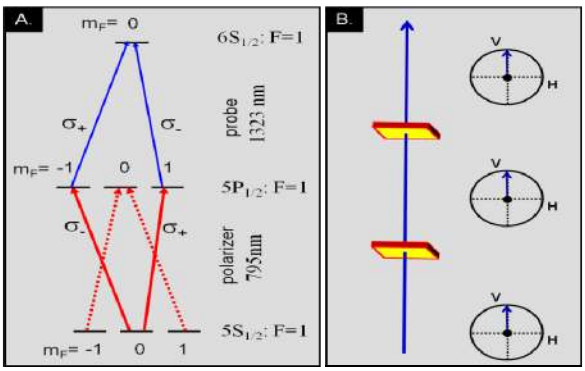

Fig. 2. Schematic illustration of an optically controlled polarizer using a ladder transition in 87Rb atoms.

In Fig. 2(a), we illustrate the basic mechanism for realizing such a polarizer, using a simplified set of transitions. We assume here that the atomic population is optically pumped into $5S_{1/2}$,F = 1,m_F = 0 Zeeman sublevel. Here, the control beam at 795 nm is resonant, and linearly polarized, in the horizontal direction, for example. This means that the two circular components of the control beam, σ_+ and σ_-, are out of phase with each other. As such, these components will produce an out-of-phase superposition of the $m_F = -1$ and $m_F = 1$ Zeeman sublevels. Such a superposition would act as a non-absorbing (dark) state for the 1323 nm probe that is vertically polarized, since it has two circular polarization components (σ_+ and σ_-) that are in phase with each other. By the same token, this superposition will act as a strong absorber for a 1323 nm probe that is horizontally polarized. Thus, the presence of this control beam would make the system an ideal polarizer. Of course, experimental conditions result in non-ideal behavior and these are discussed in later sections.

4. QZE based all-optical logic gate

A QZE based optical logic gate can be realized if the polarizing effect generator is augmented by a wave-plate effect generator, as shown in Fig. 3. Before we understand the working of the logic gate, it is instructive to understand how the waveplate effect is generated. Consider first the case where the lower leg is excited by the field which is detuned from resonance, and the fields on resonance arrows are turned off. The control field is now a right-circularly polarized (σ_+) beam at around 795 nm, tuned a few GHz below the $5S_{1/2}$,F = 1↔$5P_{1/2}$,F = 1 transition. We assume here that the atomic population is optically pumped into the $5S_{1/2}$,F = 1,m_F = 0 Zeeman sublevel. The control beam, therefore, produces an off-resonant excitations to only the $5P_{1/2}$,F = 1,m_F = 1 Zeeman sublevel in the intermediate state. The probe, at around 1323 nm, is chosen to be linearly polarized; therefore, it has two components: σ_+ and σ_-. As shown in the diagram, the σ_- component sees the effect of the atoms (because of the detuning, it sees only a real susceptibility, with virtually no absorption), while the σ_+ component does not. The parameters of the control beam can be tuned to achieve the condition for a π phase-shift for the σ_- component only, so that the polarization of the signal beam is rotated by 90 degrees. Theoretical and experimental investigations of controlled polarization rotation of a probe field using another optical field (pump) and employing ladder transitions in Rb have been carried out previously [19,20]. However, both of these employ the EIT effect where the upper leg is excited by a strong control field while the lower leg is probed by a weak optical field, and thus has fundamentally different characteristics than the system we have considered.

#194534 - $15.00 USD Received 24 Jul 2013; revised 11 Sep 2013; accepted 14 Sep 2013; published 7 Oct 2013

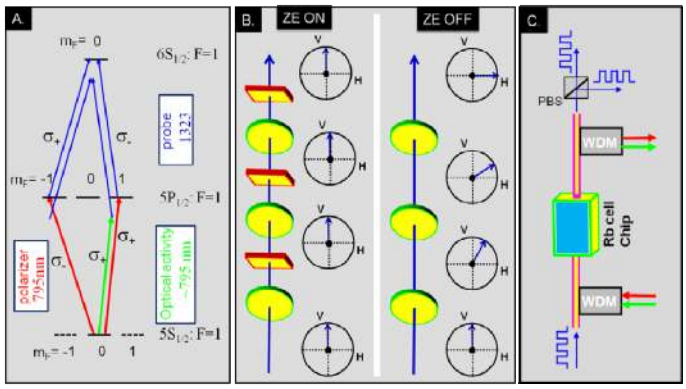

Fig. 3. Schematic illustration of an optical logic gate using a ladder-transition based polarizer and optical activity in Rb atoms.

The red beams on the lower leg represent the control signal for the polarizer. The presence of this control beam results in selective transmission of one particular polarization of the signal beam (blue) and complete suppression of the orthogonal polarization, as explained previously. In order to understand the effect of applying both the green and red control beams simultaneously, one should recall the model presented in Fig. 1 for the QZE and the discussion that followed, where we considered N pairs of polarizers and polarization rotators, and showed that the polarization does not change as $N \rightarrow \infty$. The physical implementation described here operates in this limit. Even though both processes are occurring simultaneously, the net result is equivalent to infinitesimal evolutions where the processes alternate after each time step.

When the polarizing effect generator is turned off, the polarization of the probe beam rotates by 90 degrees; when it is left on, the Zeno effect induced by the measurement due to the polarizer prevents the polarization of the probe beam from rotating, without any attenuation. This is illustrated in Fig. 3(b). On the other hand, when the waveplate effect generator is turned off, the polarization state does not change at all. In Fig. 3(c), we show how this process can be used as an optical logic gate for a probe data stream. Briefly, using WDM couplers, all the control beams and the probe at 1323 nm are made to propagate through a Rb $^{\text{vapor}}$ cell. Another WDM coupler is used to filter out the beams at 795 before the final polarizing beam splitter (PBS) placed at the output. The two ports of the PBS serve as the two output channels of the gate. If the control beams represent a data stream with their presence and absence denoting the '1' and '0' state respectively, then it is easy to construct a truth table for the outputs at port 1 and 2 respectively as shown in Table 1.

Table 1. Truth table for QZE based logic gate

Polarizer	Waveplate	O/P at Port 1	O/P at Port 2
0	0	1	0
0	1	0	1
1	0	1	0
1	1	1	0
X	Y	X + Y'	X'Y

Thus, if the sense of the '1' and '0' states of the waveplate effect generator beam are reversed, output at port 1 simply implements an OR operation on the 2 inputs while if the same is done for the polarizer effect generator, output at port 2 implements an AND gate. Of course, the output at ports 1 and 2 are complementary, as expected for a PBS. Full implementation of such a logic gate requires the realization of both the polarizer effect and

#194534 - $15.00 USD Received 24 Jul 2013; revised 11 Sep 2013; accepted 14 Sep 2013; published 7 Oct 2013

the waveplate effect in the same medium. However, given the complexity offered by an actual atomic system, we decided to investigate and optimize these two effects separately. In another paper, we present the details of our study of the waveplate effect. In this paper, we describe the details of our study of the optically controlled polarizer.

5. Stokesmetric imaging

It is well documented that in many situations of interest, features indiscernible via conventional imaging become highly resolved under Stokesmetric Imaging (SI) [21–24]. In a typical SI scenario, a target is illuminated by fully or partially polarized light. The light scattered or reflected by the target is then analyzed using a Stokesmeter, which determines the magnitude of each of the four Stokes parameter components. Stokesmeters, in their simplest form, are comprised of a combination of polarizers and wave-plates with different orientations. A key problem with the existing SI systems is that the polarizers and waveplates cannot be turned on or off or reoriented rapidly. The free space versions of the optically controlled polarizers and waveplates that are described in this paper have the potential to operate at speeds of few MHz (limited by the decay rate of the intermediate level) and thus hold the promise of making very high speed SI practical.

6. Experimental set-up

The experimental configuration we used to realize an optically controlled polarizer is shown is shown schematically in Fig. 4. We used a conventional vapor cell, containing a natural mixture of both the isotopes of Rb. However, we used only ^{87}Rb for our experiment. Here, the control beam and signal beam are co-propagating. A similar set-up was used when the control beam and the signal beam were counter-propagating.

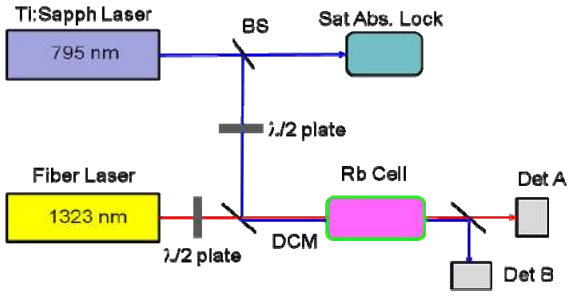

Fig. 4. Experimental setup used to realize the ladder-sysetm polarizer.

Briefly, beams from two tunable lasers (one at 795 nm, and the other at 1323 nm) were combined with a dichroic mirror (DCM). A part of the 795 nm light was sent to a reference vapor cell for saturated absorption spectroscopy and locking. The combined beams were sent through a vapor cell, shielded from magnetic fields with μ-metal. The cell was heated using bifiliarly wounded wires that do not add any magnetic fields. After passing through the cell, another DCM was used to split the light into two parts, and each frequency was detected with a separate detector. The polarization of each input beam was controlled separately with two half waveplates. The control laser was locked to one of the lines on the $5S_{1/2}$, $\leftrightarrow 5P_{1/2}$ manifold, while the signal laser at 1323 was scanned over the $5P_{1/2} \leftrightarrow 6S_{1/2}$ manifold. For the remainder of the paper, the hyperfine levels in the ground state are indicated by unprimed alphabets (F), those in the $5P_{1/2}$ level are primed (F') and those in the $6S_{1/2}$ level are double-primed (F").

In section 3, we showed a simplified set of energy levels in order to explain the basic process behind an optically controlled polarizer. In practice, however, it is extremely difficult to realize such an ideal system. For example, it is generally necessary to take into account

#194534 - $15.00 USD Received 24 Jul 2013; revised 11 Sep 2013; accepted 14 Sep 2013; published 7 Oct 2013

both the hyperfine levels (F' = 1 and F' = 2) in the $5P_{1/2}$ manifold to account for Doppler broadening and power broadening. Furthermore, it is virtually impossible to eliminate all the atoms from the $m_F = \pm 1$, F = 1 Zeeman sublevels via optical pumping. Hence, all the Zeeman sub-levels at the $5P_{1/2}$ manifold also get coupled with the optical fields. The full set of relevant energy levels that need to be considered are shown in Fig. 5. In our model, we considered all the Zeeman sub-levels which explicitly interact with an optical field (all sub-levels of the F=1, F'=1,2 and F"=1,2 hyperfine levels), while the F = 2 hyperfine level and the $5P_{3/2}$ level were only considered as population transfer levels and hence all their sub-levels were lumped together as a single level. The transition strengths [25] indicated are expressed as multiples of the weakest transition, which in our case is the transition from the F = 1, m_F = 1 sub-level to the F' = 1, m_F = 0 sub-level. In order to avoid unnecessary clutter, the matrix elements for the F' = 1 to F" = 1, 2 transitions and for the F' = 2 to F" = 1 transition are not shown. More details regarding the model are presented in the section 8. Initially, we carried out our experiments without employing optical pumping. Later in the paper, we will discuss in detail how to implement optical pumping properly in order to optimize the performance of the polarizer.

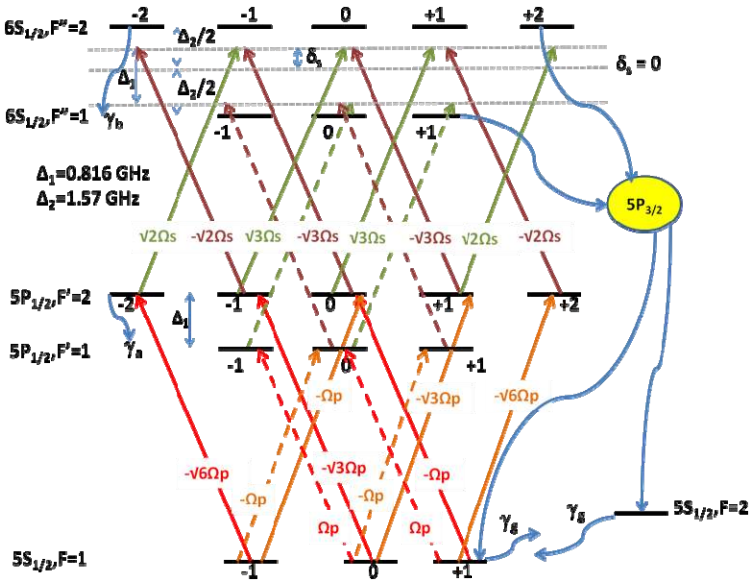

Fig. 5. Model used for numerical computation. See text for more details.

7. Results

Figure 6(a) shows evidence of the polarizing property of the control beam as the signal beam was scanned across the $5P_{1/2} \leftrightarrow 6S_{1/2}$ manifold. The control beam was vertically polarized, co-propagating with the signal beam, had a power of ~5mW and was locked to the F = 1→F' = 2 line. The temperature of the cell was about ~200 Celsius. The blue (red) trace is the signal transmission when the signal beam is vertically (horizontally) polarized. The F" = 1 and F" = 2 labels indicate the transitions from the F' = 2 level, as the power of the control beam was not strong enough to produce excitations to the far detuned F' = 1 level. As is evident from Fig. 6(a), signal transmission for the F' = 1→F" = 1 increased significantly when the control beam and the signal beam are cross-polarized. The F' = 1→F" = 2 transition showed opposite behavior to the F' = 1→F" = 1 line in terms of the percentage of absorption. This is due to the fact that the matrix elements for the σ_- transitions of the F' = 2 → F" = 2 line are of opposite sign as compared to the F' = 2 → F" = 1 line [25], and hence the σ_- coherences pick up an

#194534 - $15.00 USD Received 24 Jul 2013; revised 11 Sep 2013; accepted 14 Sep 2013; published 7 Oct 2013

additional phase difference of π, thus changing the sense of polarization from horizontal to vertical and vice-versa. The assumption in the preceding argument is that the significant contribution to the absorption of the signal beam is from the F' = 2 level, since the F' = 1 is highly detuned.

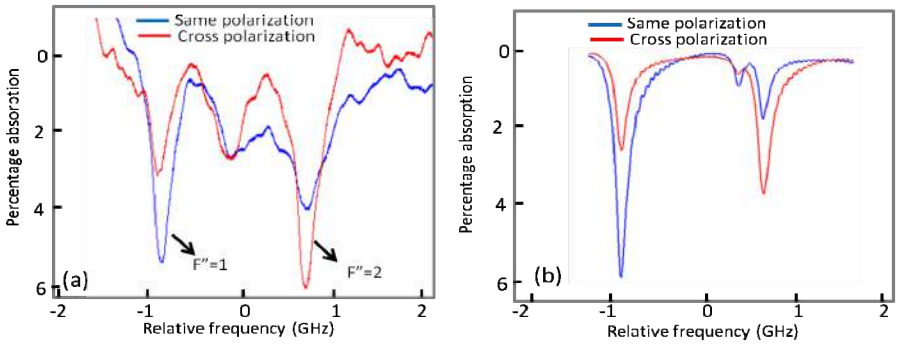

Fig. 6. Polarizer effect for co-propagating geometry for pump power ~5mW a) Experiment b) Theory.

We obtain ~50% reduction in absorption for the F' = 2 → F" = 1 line and about ~70% reduction for the F" = 2 line. The background modulation is due to an etalon effect caused by the two windows of the cell, which were anti-reflection (AR) coated for 795 nm, but not for 1323 nm. In the future, the etalon effect could be eliminated by using a cell where the windows are not parallel to each other, along with AR-coating at 1323 nm. Figure 6(b) shows the corresponding numerical simulation and it is fairly consistent with our experimental result. For this particular simulation, the pump was slightly detuned below the F = 1→F' = 2 line and this results in the appearance of an additional dip near the F" = 2 line, which is due to the F' = 1→F" = 2 line. Indeed, this feature does not appear if the pump laser is resonant with the F = 1→F' = 2 line or if the pump power is not sufficient to excite the atoms to the F' = 1 level. In the experimental data too there seems to be an additional dip in-between the two lines, which we believe may not be caused due to the etalon effect alone. As our simulations indicate, this additional feature might be due to a shift in the pump laser frequency resulting in excitations from the F' = 1 level, but a more thorough investigation is needed to resolve this apparent discrepancy. However, it should be noted that the device we propose would operate at one of the main absorption dips, rendering the central dip largely irrelevant.

We also investigated the performance of the polarizer under a counter-propagating geometry. Figure 7 shows data for the F" = 1 transition obtained for two different power levels (~2mW and ~200mW) of the control beam and the corresponding numerical simulation. The F" = 2 transition also showed similar behavior and is not shown here for the sake of brevity.

#194534 - $15.00 USD Received 24 Jul 2013; revised 11 Sep 2013; accepted 14 Sep 2013; published 7 Oct 2013

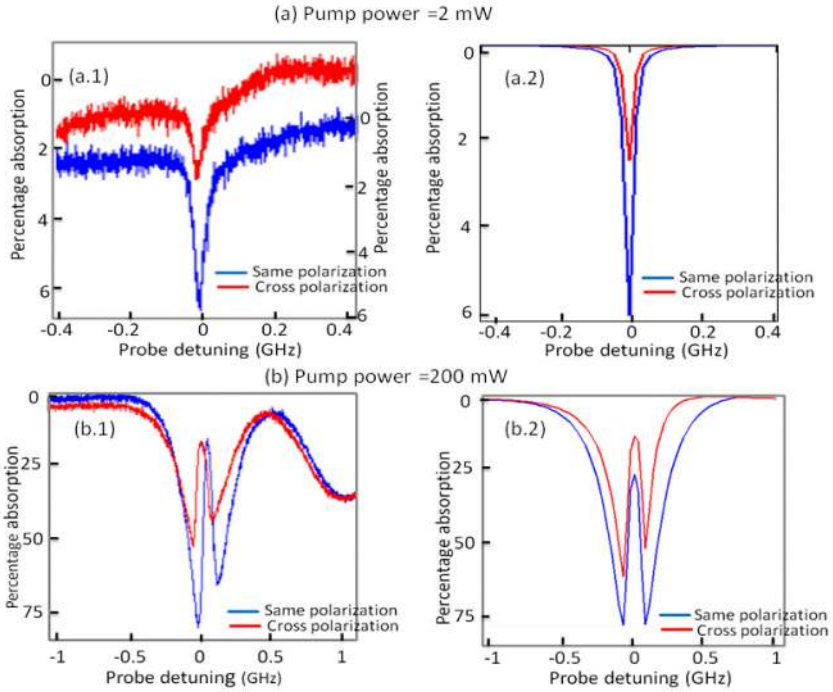

Fig. 7. Polarizer effect for counter-propagating geometry for 2 different powers of the pump. a.1) Experiment a.2) Theory and b.1) Experiment b.2) Theory.

It is useful to note a couple of differences in the observed signals between the co-propagating and the counter-propagating cases. Since we do not have experimental data under identical conditions (powers of the pump and the probe, temperature etc.) for the two geometries and our theoretical results are fairly consistent with our experimental data, we would present these differences using our simulation results. Figure 8 shows the simulation results for both geometries for a pump Rabi frequency of 5 (in units of the natural linewidth of the 5P manifold ~5.7 MHz) when both the control and the signal beams have the same polarization. As seen in Fig. 8, the counter propagating geometry produces narrower (and deeper) absorption lines as compared to the co-propagating case. In addition, there is also an apparent splitting in the counter-propagating geometry which is absent in the co-propagating case. These differences based on geometry are due to what we refer to as pump power limited Doppler broadening (PPLDB) but we believe this issue is tangential to the focus of the work presented here and hence we discuss it in greater detail in the appendix.

#194534 - $15.00 USD Received 24 Jul 2013; revised 11 Sep 2013; accepted 14 Sep 2013; published 7 Oct 2013

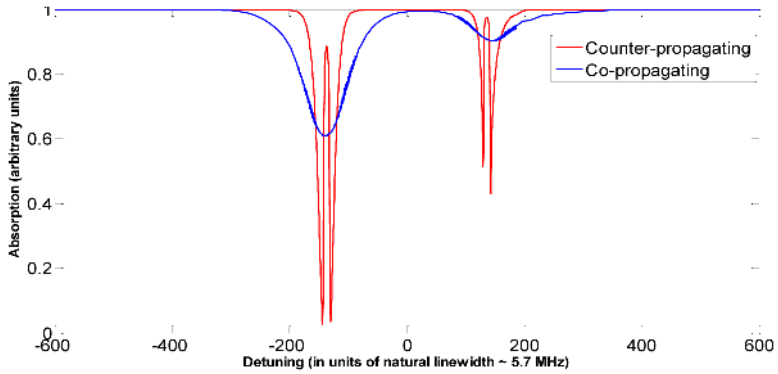

Fig. 8. Typical absorption profile for co- and counter-propagating geometries. Here, $\Omega_p = 5$.

Despite the significant differential absorption at virtually all power levels of the 795nm light, in order for our system to work as an ideal polarizer, we need nearly 100% suppression of one polarization versus nearly 100% transmission for the orthogonal polarization. Towards this end, we used our numerical model to identify the parameter space and experimental modifications needed to improve the contrast. We will first describe the model used before going to discuss the experimental modification necessary to achieve an acceptable contrast in probe absorption.

8. Model used for simulation and computational details

Any analysis of the polarizer proposed above would require careful monitoring of the populations and coherences of the various Zeeman sub-levels involved in the system. A detailed diagram of all the relevant levels considered along with the relative transition strengths has been presented in Fig. 5. Due to power broadening, the $5P_{1/2}$, F' = 1 hyperfine level interacts with both the control and the signal optical fields (indicated by dashed lines), albeit at a large detuning, and these interactions have been taken into account in our model. However, we ignored the coherent coupling between F = 2 and the $5P_{1/2}$ manifold, because of the large frequency difference between F = 1 and F = 2 (~6.8GHz for ^{87}Rb). Also, while the control beam is shown to be resonant in Fig. 5, ours is a general model where the control beam can be detuned from the F' = 2 level by an arbitrary value, say δ_p.

All the Zeeman sub-levels in the $5P_{1/2}$ ($6S_{1/2}$) manifold are assumed to decay at the same rate, γ_a~5.75 MHz (γ_b~3.45 MHz). We also assume a nominal cross-relaxation rate (γ_g ~0.1 MHz) between F = 1 and F = 2 hyperfine levels. Figure 9 shows the various decay channels and branching ratios in the system. Here, the individual decay rates between the Zeeman sub-levels are not explicitly shown but only the branching ratios between the hyperfine levels, which were obtained by summing the decay rates of all possible transitions between the corresponding hyperfine levels. The decay rate between any two Zeeman sub-levels was calculated by assuming it to be proportional to the square of the matrix element of the corresponding transition, such that the sum of all such decays rates from the decaying level equaled the net decay from that level. For example, consider $m_F = 0$, F' = 2 sub-level which decays at a rate γ_a. The transition strengths for the σ_+, σ_-, and π-transitions to the F = 1 (F = 2) are in the ratio 1:1:2 ($\sqrt{3}$:$\sqrt{3}$:0). Thus, the net decay rate between the $m_F = 0$, F' = 2 sub-level to the $m_F = -1$, + 1 and 0 states of the F = 1 level were computed to be $\gamma_a/12$, $\gamma_a/12$ and $\gamma_a/3$ respectively and the decay to the F = 2 level was computed to be $\gamma_a/2$, since all the hyperfine levels in the F = 2 state are lumped together as a single state in our model. We have also taken into account the sourcing of atoms into the ground states from the $6S_{1/2}$ state via the $5P_{3/2}$ state (shown by dashed lines in Fig. 9). For our computations, these additional source terms were modeled using an "effective decay rate" directly from the hyperfine levels in the $6S_{1/2}$ state to the $5S_{1/2}$ manifold. A detailed calculation, taking into account the various branching ratios

#194534 - $15.00 USD Received 24 Jul 2013; revised 11 Sep 2013; accepted 14 Sep 2013; published 7 Oct 2013

into and from all the hyperfine levels of the $5P_{3/2}$ state was used to determine these rates. However, the decay rate of each of the individual Zeeman sub-level in the $6S_{1/2}$ state was not considered, rather it was assumed that all of them decayed equally to the Zeeman sub-levels of F = 1 and F = 2 levels at the respective "effective decay rates" previously determined. The ratio between the decay rates into the $5P_{1/2}$ and $5P_{3/2}$ state from the $6S_{1/2}$ state was simply decided by the ratio of the explicit values of the transition strength of the D1 and D2 lines [25].

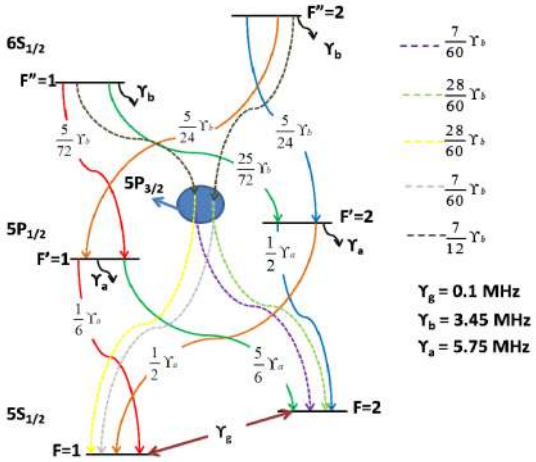

Fig. 9. Decay rates and branching ratios between various levels in our model.

In addition to keeping track of the signs of the matrix elements involved in the transitions between the Zeeman sub-levels, it is also important to keep track of the explicit phase associated with the optical fields. In most cases, this phase can be factored out while transforming the Hamiltonian to the rotating basis. However, if any level has multiple pathways for excitation such that the pathways form a closed loop architecture, it is not possible to transform all the phases out of the Hamiltonian. Upon transformation to the rotating basis, this results in the appearance of a so called "closed-loop phase" on one of the legs of the Hamiltonian which cannot be eliminated by any transformation, as shown in Fig. 10. In fact, changing the polarization of either the signal beam or the control beam from horizontal to vertical results in changing this closed-loop phase by π and thus the study of the Polarizer effect essentially boils down to studying the behavior of the system as this closed-loop phase is switched between 0 and π.

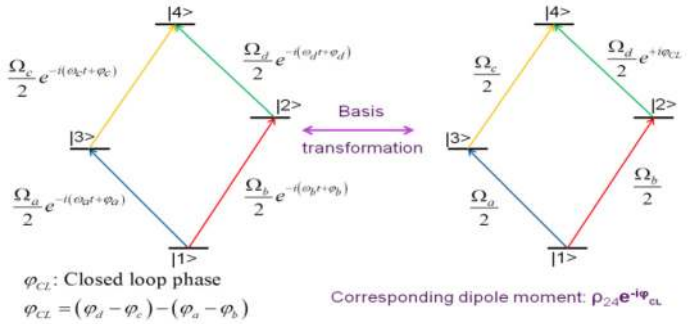

Fig. 10. Effect of closed-loop architecture resulting from multiple excitation pathways between two levels.

#194534 - $15.00 USD Received 24 Jul 2013; revised 11 Sep 2013; accepted 14 Sep 2013; published 7 Oct 2013

In our model, we have up to a maximum of 20 levels. We used the Liouville equation, that describes the evolution of the density matrix in terms of a commutator between the density matrix and the Hamiltonian, to obtain the steady-state solution. The usual method of vectorizing the density matrix and then inverting the coefficient matrix thus obtained, is not easy to handle as the size of the coefficient matrix is very large (400*400). In order to overcome this problem, we developed a novel algorithm which would compute the said coefficient matrix automatically, given the Hamiltonian and the source matrix. Briefly, we set each of the elements of the density matrix to unity one at a time while setting all the others to zero and repeatedly compute the commutator between the density matrix and the Hamiltonian. Once this procedure is repeated over all the elements of the density matrix, we would have computed the coefficient matrix. The source terms, as well as any other dephasing terms (such as collisional dephasing) are added in finally as a constant matrix. Details regarding the algorithm are to appear in a separate paper, which is currently under review [26].

While averaging over the Doppler profile, we used the supercomputing cluster at Northwestern (QUEST) to perform our computations. Using 64 cores and computing the steady state solution for 512 values of detuning, each averaged over 800 points of the Doppler profile, we obtained the steady-state solution for our 20-level system in 3-4 minutes. With a smaller system, say for a 15-level system, we obtained the solution in a few seconds. Some of the results, thus obtained, have already been reproduced in Section 6. For all the simulations, a temperature of 500 Kelvin was used and the density of atoms was taken to be $\sim 10^{11}/cm^3$

9. Improvements to system and future work

In general, the quality of a polarizer is characterized by its extinction ratio, η, defined as the ratio of the transmitted intensity of light with its state of polarization (SOP) parallel to the transmission axis to the transmitted intensity of the same beam of light with its SOP perpendicular to the transmission axis. The minimum value of η that might be acceptable depends on the signal to noise ratio (SNR) desired in a particular application. For the SI application, for example, an SNR of about 5 would suffice, according to the Rose criterion [27]. For the optical logic gate, the SNR requirement could be even lower. This would translate directly to the η that can be achieved in our polarizer, assuming other sources of noise are negligible. The best case, shown in Fig. 7(b) corresponds to an $\eta \sim 2.5$. The value of η can be increased significantly by using higher optical densities of the Rb medium (resulting in very high absorption of light polarized perpendicular to the transmission axis) but this would also result in lowering of the transmission of light polarized along the transmission axis of the polarizer. Thus, the requirement of a high value of η needs to be balanced against maximum achievable transmission and this would again depend on the particular application at hand.

In order to increase the extinction ratio of our all-optical polarizer without sacrificing the maximum transmission achievable for a beam of light polarized along the transmission axis, it is necessary to make modifications to our system. One of the non-idealities in our system is that all the Zeeman sublevels in the F = 1 state are populated due to decay from various channels. Since the transition between the $F = 1, m_F = 0$ and the $F' = 1, m_F = 0$ Zeeman sublevels is forbidden, application of a π-polarized optical pumping beam between the F = 1 and F' = 1 states would pump the atoms into the $F = 1, m_F = 0$ state, as required. However, we note that a π-transition is allowed between the $F = 1$, $m_F = 0$ and $F' = 2$, $m_F = 0$ Zeeman sublevels. Hence, if the interaction of the π-beam with F' = 2 in considered, it is not possible to obtain a time-independent Hamiltonian after switching to a rotating basis. In order to circumvent this complication, we made the simplifying assumption that the π-beam excites only the $F = 1 \rightarrow F' = 1$ transition. Although not necessary, we also assumed that the control beam only interacts with the F' = 2 level. Given the separation (0.816 GHz) between the F' = 1 and F' = 2 levels, these assumptions are valid for the power levels used in our simulation, as

#194534 - $15.00 USD Received 24 Jul 2013; revised 11 Sep 2013; accepted 14 Sep 2013; published 7 Oct 2013

detailed later. The π-beam, expanded using a cylindrical lens and locked to F = 1→F' = 1 transition, needs to be brought in through a slot running parallel to the length of the Rb Cell.

However, application of this pumping beam alone is not sufficient, as there is decay from the intermediate (5P) levels into the F = 2 state, which is another non-ideality in our system. This mandates the need for another optical pumping beam from the F = 2 state to the $5P_{3/2}$ state. The net effect of this additional pumping beam was modeled as an increased decay rate from the F = 2 to F = 1 state. The maximum decay rate obtainable by the application of such a beam is γ_a, the radiative decay rate of the $5P_{3/2}$ manifold. We further note that the ratio of steady-state populations in the F = 1 and F = 2 states (in the absence of any field) can be estimated to be $\sim\gamma_a/\gamma_g$, where γ_g is the nominal decay rate from the F = 1 to F = 2 state. It is clear that we can increase the population in the F = 1 state by further decreasing γ_g, and this can be accomplished by using a buffer gas loaded cell. Figure 11 shows our model after the afore-mentioned changes are incorporated. As noted previously, to avoid unnecessary clutter, not all transition strengths are shown.

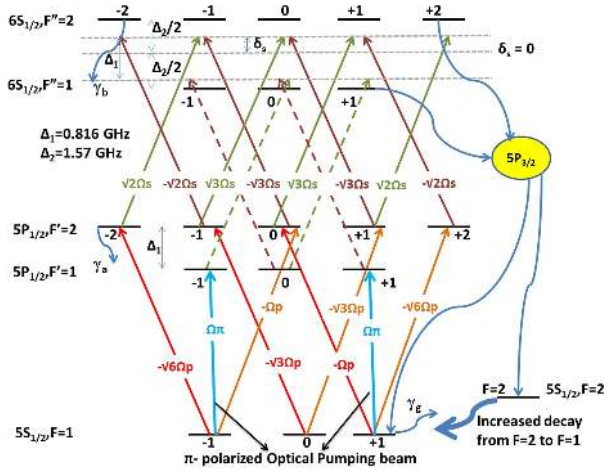

Fig. 11. Modified model after addition of optical pumping beams and buffer gas.

A typical simulation result obtained by employing the modified system is shown in Fig. 12. Again, only the F' = 2→F" = 1 transition is shown for the sake of brevity. As is evident from Fig. 12, at zero detuning, a signal beam with the same polarization as the control beam is almost completely absorbed (0.00001% transmission) while nearly 90% of an orthogonally polarized beam is transmitted, corresponding to an $\eta\sim10^5$, comparable to the best commercially available polarizers. For this particular simulation, we used the co-propagating geometry, the decay rate from the F = 2 to F = 1 state was set to be equal to the decay rate of the 5P manifold while the decay rate in the opposite direction was set (reduced due to buffer gas) to about 10 KHz. The Rabi frequencies of the control beam and the optical pumping beam were set to be 0.5 and 10 (in units of the natural linewidth of the 5P manifold γ_a ~5.7 MHz), respectively. The density of atoms was taken to be $10^{11}/cm^3$ and the temperature was set to 500K.

#194534 - $15.00 USD Received 24 Jul 2013; revised 11 Sep 2013; accepted 14 Sep 2013; published 7 Oct 2013

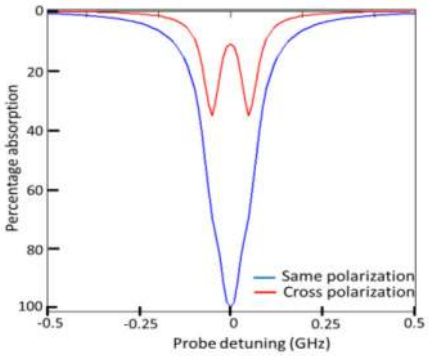

Fig. 12. Numerical simulation of polarizer effect in the presence of two optical pumping beams and using a buffer gas loaded cell.

It should be possible to realize such a polarizer at a very low light level, using a tapered nanofiber (TNF) embedded in Rb vapor [6,9–11]. In a TNF, the typical mode area is ~0.2 μm^2 [9]. Thus, assuming a saturation intensity of 3mW/cm^2, a Rabi frequency of $10\gamma_a$ would correspond to a power of only ~1 nW. Unlike the free space case, the maximum speed of operation in the TNF system would be limited by the transit time broadening (~60 MHz) rather than the natural linewidth of the 5P manifold (~6 MHz). To see why, note that the speed is limited by the rate at which atoms in the intermediate state relax to the ground state [7] and for a TNF system, this rate is effectively determined by the transit time. Finally, we note that the TNF system may be suitable only for demonstrating an all-optical logic gate but not for SI, for which the free space version of the polarizer is better suited. Significant changes to the set-up are required in order to implement the improved scheme both in free space and in the TNF system. Efforts are underway in our laboratory towards making these modifications and we intend to report on the progress and results in the near future.

10. Conclusions

To summarize, we have demonstrated an optically controlled polarizer at ~1323 nm using a ladder transition in a Rb vapor cell. We investigated two geometries – when the control and the signal beams are co-propagating and counter propagating. We find that the signal beam shows significant differential absorption (50-70%) when the control beam is polarized in the same direction, and when it is cross-polarized. The process is a manifestation of constructive and destructive interference of the coherences between various Zeeman sub-levels. We identified differences in the performance of the system for co-propagating and counter-propagating geometries. We also modeled the system including most of the Zeeman sub-levels in the problem and our numerical simulations agree quite well with experiments. A novel algorithm was used to obtain the steady state solution for such a large quantum system. We have also identified means to improve the contrast in the absorption and efforts are underway in our laboratory to incorporate these changes. In addition, we describe how such a polarizer, combined with an optically controlled waveplate, recently demonstrated by us, can be used to realize an ultra-low power, high speed all-optical logic gate, based on the Quantum Zeno Effect, for the telecom band using a tapered nanofiber embedded in a vapor cell.

11. Appendix

Here, we address the issue of the differences in line shapes between co- and counter-propagating geometries, as shown in Fig. 8. For the purpose of understanding, it suffices to consider a 3-level cascade system with similar energy difference between the levels as in our original system i.e $k_2 \sim 0.6\ k_1$. Figure 13(a) shows such a system where the pump is on resonance with the intermediate level and the probe is scanned across the upper level. Figure

#194534 - $15.00 USD Received 24 Jul 2013; revised 11 Sep 2013; accepted 14 Sep 2013; published 7 Oct 2013

13(b) shows the (partial) dressed picture of the interactions for the zero velocity atoms. Here |1'> and |2'> are shown to be degenerate (with δ_p=0), while we show |3> to be higher in energy by an amount equal to probe field energy (for δ_s=0). This picture is valid for a weak probe and enables us to understand clearly the dynamics of the probe absorption. On the right-side of Fig. 13(b), we show the two split states that result from diagonalization of the interaction between |1'> and |2'>. Similar diagrams are shown in Figs. 13(c) and 13(d) for a positive velocity (same direction of propagation as pump) for the co- and counter-propagating configurations, respectively.

For an arbitrary velocity group v, the energies of the partially diagonalized states can be easily calculated to be $\lambda = \left(-k_1 v \pm \sqrt{(k_1 v)^2 + \Omega_p{}^2}\right)/2$, where k_1 is the wavevector of the pump optical field and Ω_p is the pump Rabi frequency. Thus, for the zero-velocity group of atoms, these atomic states would have energies $\pm\Omega_p/2$ and hence would produce absorption at probe detunings of $\mp\Omega_p/2$, as shown in Fig. 13(b). This is a manifestation of the well-known Autler Townes splitting (ATS). For any non-zero velocity group, the probe would be further Doppler shifted by $k_2 v$, with the direction of shift depending on whether the probe is co- or counter-propagating, as shown in Figs. 13(c) and 13(d) respectively. Thus, the resonances would occur at $\left(k_2 + \frac{k_1}{2}\right)v \mp \sqrt{(k_1 v)^2 + \Omega_p{}^2}/2$ for a co-propagating probe and at $\left(k_2 - \frac{k_1}{2}\right)v \mp \sqrt{(k_1 v)^2 + \Omega_p{}^2}/2$ a counter-propagating probe. We also note that the velocity spread of atoms that contribute significantly to the absorption can be estimated to be of the order of $kv_{FWHM} \sim \sqrt{r_2{}^2 + 2\Omega_p{}^2}$ where Γ_2 is the decay rate of the intermediate level. From these expressions, we can make the following observations:

a) For a vanishingly weak pump, the spread of the velocity groups that contribute significantly to the absorption of the probe is very small ($kv_{FWHM} \sim \Gamma_2$). Thus, both geometries would produce narrow lines (although co-propagating is still slightly broader) with linewidths that are essentially Doppler free and primarily determined by the decay rates of the intermediate and upper level. We can roughly estimate the minimum observable linewidth to be $\sqrt{r_2{}^2 + r_3{}^2}$, where Γ_3 is the decay rate of the upper level.

#194534 - $15.00 USD Received 24 Jul 2013; revised 11 Sep 2013; accepted 14 Sep 2013; published 7 Oct 2013

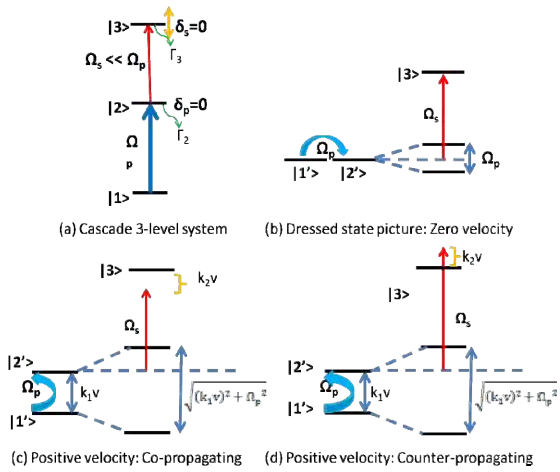

Fig. 13. Dressed state picture of 3-level cascade system for different velocity groups

b) There are some differences that arise for a pump Rabi frequency that is much larger than the minimum observable linewidth. We first note that in the co-propagating case, for any given pump Rabi frequency Ω_p we can always find a velocity group, $v_{zero} = \Omega_p / 2\sqrt{k_2^2 + k_1 k_2}$ that produces resonance at zero probe detuning. If we carry out a similar exercise for the counter-propagating case, we find that the velocity group that produces resonance at zero probe detuning would have $v_{zero} = \Omega_p / 2\sqrt{k_2^2 - k_1 k_2}$ and this has no valid solution if $k_2 < k_1$, as is the case for our system. As a consequence, in a co-propagating geometry, ATS is generally washed out while it is preserved to some extent in the counter-propagating geometry, the specific details of which depend on the exact value of Ω_p.

c) Finally, we also note that $\left(k_2 + \frac{k_1}{2}v\right)$ is much larger than $\left(k_2 - \frac{k_1}{2}v\right)$ Thus, the resonances for the co-propagating geometry occur at much larger detunings, resulting in broader (and consequently shallower) lines as compared to the counter-propagating geometry.

Similar conclusions can be reached for the negative velocity group of atoms. We refer to this phenomenon of line broadening in a cascade system for a strong pump as Pump power limited Doppler broadening (PPLDB) since the number of velocity groups that contribute significantly to the absorption signal is proportional to the pump power. In Fig. 14, the contribution to the absorption (not normalized over the Doppler profile) from three velocity groups ($-V_{zero}$,0,$+V_{zero}$) are presented for both co-propogating and counter-propagating geometries for our simplified system. As see in Fig. 14, in the co-propagating case, the non-zero velocity groups contribute significantly to the absorption at zero detuning, while in the counter-propagating case, the contributions from non-zero velocity groups tend to align with the zero-velocity group contribution.

#194534 - $15.00 USD Received 24 Jul 2013; revised 11 Sep 2013; accepted 14 Sep 2013; published 7 Oct 2013

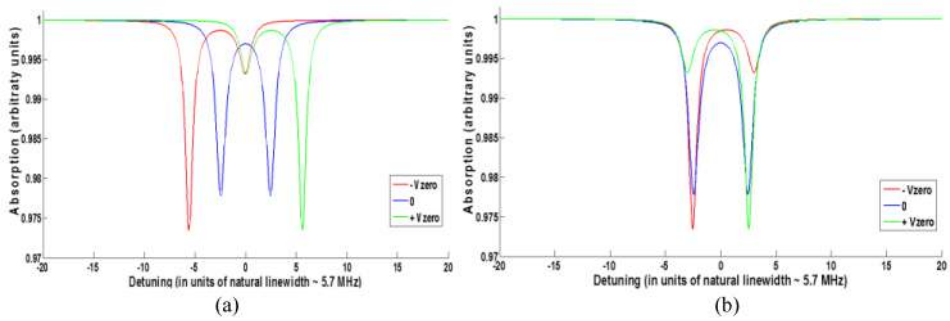

Fig. 14. Contribution to absorption from 3 sample velocity groups ($-v_{zero}$,0, + v_{zero}) for a 3-level cascade system when the control beam and signal beam are a) Co-propagating b) Counter-propagating

Of course, our original system involving all the Zeeman sublevels is more complicated due to the presence of additional levels and the fact that Rabi frequencies for the various transitions are not identical, but the intuition developed above using a simplified 3-level cascade system remains valid. In Fig. 15, the contribution to the absorption of the F"=1 line from 3 velocity groups (-u/10, 0, +u/10, where u is mean velocity of atoms) are shown for our original system (see Fig. 5) under both geometries.

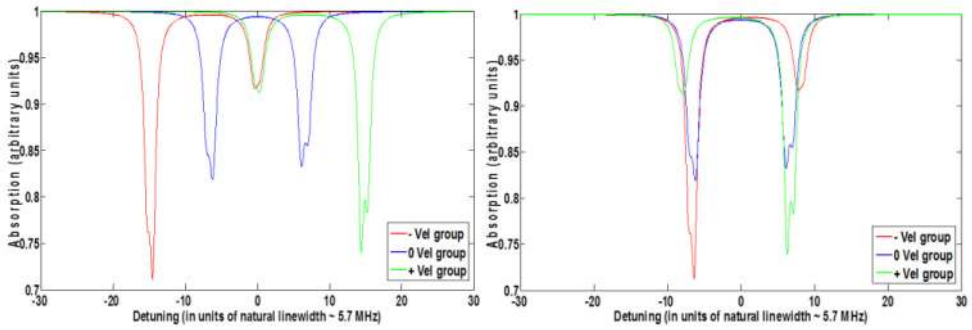

Fig. 15. Contribution to absorption of F" = 1 line from 3 sample velocity groups (-u/10,0, + u/10 where u is the mean velocity of Rb atoms) for our original cascade system (see Fig. 5) when the control beam and signal beam are a) Co-propagating b) Counter-propagating

But for the slight asymmetry in the line shapes and the appearance of some additional structure in each of the individual lines (due to the presence of multiple levels), the basic features remain identical to that of the simplified 3-level system allowing us derive the same conclusions. Thus, in a co-propagating geometry, the absorption lines are broader, shallower and the ATS is usually washed out while in a counter-propagating geometry the lines are narrower, deeper and ATS is generally preserved in the counter-propagating case, as was seen in Fig. 8.

Acknowledgments

This work was supported in part by AFOSR Grant # FA9550-10-01-0228, and the DARPA ZOE program under Grant # W31P4Q-09-1-0014.

#194534 - $15.00 USD Received 24 Jul 2013; revised 11 Sep 2013; accepted 14 Sep 2013; published 7 Oct 2013